Applied Catalysis B: Environmental 200 (2017) 330–342

Contents lists available at ScienceDirect

Applied Catalysis B: Environmental

journal homepage: www.elsevier.com/locate/apcatb

Hierarchical assembly of graphene-bridged Ag_3PO_4/Ag/$BiVO_4$ (040) Z-scheme photocatalyst: An efficient, sustainable and heterogeneous catalyst with enhanced visible-light photoactivity towards tetracycline degradation under visible light irradiation

Fei Chen[a,b], Qi Yang[a,b,*], Xiaoming Li[a,b], Guangming Zeng[a,b], Dongbo Wang[a,b,*], Chenggang Niu[a,b], Jianwei Zhao[a,b], Hongxue An[a,b], Ting Xie[a,b], Yaocheng Deng[a,b]

[a] College of Environmental Science and Engineering, Hunan University, Changsha 410082, PR China
[b] Key Laboratory of Environmental Biology and Pollution Control (Hunan University), Ministry of Education, Changsha 410082, PR China

ARTICLE INFO

Article history:
Received 3 May 2016
Received in revised form 4 July 2016
Accepted 16 July 2016
Available online 18 July 2016

Keywords:
Visible light photocatalyst
Graphene-bridged Ag_3PO_4/Ag/$BiVO_4$
Tetracycline
Synergistic effect
Photostability

ABSTRACT

A novel graphene-bridged Ag_3PO_4/Ag/$BiVO_4$ (040) Z-scheme heterojunction with excellent visible-light-driven photocatalytic performance was fabricated using a facile in situ deposition method followed by photo-reduction. The as-obtained nanocomposite was employed to degrade tetracycline (TC) in water under visible light irradiation. Compared to pure $BiVO_4$, Ag_3PO_4 and other nanocomposites, Ag/Ag_3PO_4/$BiVO_4$/RGO displayed more superior photodegradation efficiency with 94.96% removal of TC (10 mg/L) in 60 min, where the optimal conditions was catalysis dosage 0.50 g/L and initial pH at ca. 6.75. The influences of TC concentrations, light irradiation condition, coexistence ions and water sources were also investigated in details. The enhanced photocatalytic activities could be attributed to the suppression of charge recombination, high specific surface area and desirable absorption capability of Ag/Ag_3PO_4/$BiVO_4$/RGO, which were in sequence confirmed by PL, PC, EIS, BET and DRS tests. The synergistic effects of RGO and Ag/Ag_3PO_4 in the hybrid could also contribute to the improved photo-stability and recyclability towards TC decomposition. In addition, radical trapping experiments and ESR measurement revealed that the photo-induced active species superoxide radical ($^{\bullet}O_2^-$) and holes (h^+) were the predominant active species in the photocatalytic system. The Ag/Ag_3PO_4/$BiVO_4$/RGO nanocomposite also possessed desirable photocatalytic performance on the degradation of TC from real wastewater, further verifying its potential in practical industries. This work provides a promising approach to construct visible-light response and more stabilized nanocomposite photocatalysts applied in efficient treatment of persistent pollutants in wastewater.

1. Introduction

Over the past decades, the presence of antibiotics (persistent organic pollutants) in water has raised considerable concerns because of the unknown environmental impacts and possible damages to the botany and fauna in aquatic system [1,2]. As a typical antibiotic, tetracycline (TC) has been extensively used in a variety of human, veterinary and farming applications [3–5], which might pose serious threats to the ecosystem and human health when entered into aqueous environments. TC has been detected in different waters such as surface water, groundwater and even drinking water [6–8]. The removal of antibiotics including TC from the environment has already become a mandatory issue.

A large number of techniques have been employed to remove TC from water, including absorption, electrolysis, photocatalysis, microbial decomposition and membranes separation etc. [9,10]. Among them, photocatalytic degradation of TC was presented as a desirable approach due to its high efficiency, high-efficient energy conservation and low cost. However, the application of most frequently used TiO_2-based photocatalyst was limited by its low adsorption capacity for hydrophobic pollutants and inef-

* Corresponding authors at: College of Environmental Science and Engineering, Hunan University, Changsha 410082, PR China.
E-mail addresses: feichen@hnu.edu.cn (F. Chen), yangqi@hnu.edu.cn (Q. Yang), w.dongbo@yahoo.com (D. Wang).

http://dx.doi.org/10.1016/j.apcatb.2016.07.021
0926-3373/

ficient exploitation of abundant visible light in the solar irradiation [11,12]. Accordingly, it is necessary to search new-type photocatalysts for the effectively degradation of TC under visible light irradiation. Recently, the monoclinic bismuth vanadate (m-$BiVO_4$) has been widely studied in the field of visible-light photocatalysis owing to its narrow bandgap (about 2.4 eV), sufficient photocatalytic response and chemical stability [13]. Nevertheless, the photoactivity of pure $BiVO_4$ is still not satisfactory, attributing to its poor migration efficiency of electron-hole pairs and weak surface adsorption properties [14]. The heterojunction construction has been proved to be a good choice to enhance the photocatalytic performance, with successful cases such as $BiVO_4/Bi_2S_3$ [15], $Cu_2O/BiVO_4$ [16], $BiVO_4/TiO_2$ [17], $Ag_3PO_4/BiVO_4$ [18] and so on. Li and his co-workers successfully designed $Ag_3PO_4/BiVO_4$ heterojunction photocatalyst via a simple in-situ chemical deposition method and the catalyst exhibited a perferable removal efficiency towards methyl blue (MB). For Ag_3PO_4-based photocatalysts or other common heterojunctions, an issue regarding the transfer route of photo-excited charges in the photocatalytic system still persists, where electrons or holes left on the semiconductors might easily recombine with the holes or electrons [19–21]. As a result, the emergence of Z-scheme heterojunction could solve above problem to a certain degree. For example, Bu et al. utilized in situ reduction of Ag^+ into Ag on the surface of Ag_3PO_4/WO_{3-x} to form a new-type Z-scheme heterojunction $Ag_3PO_4/Ag/WO_{3-x}$, which effectively prolonged the lifetime of photo-generated electrons by Ag_3PO_4 and photo-induced holes generated by WO_{3-x}, and therefore improved the photocatalytic degradation performance [22]. Li et al. also successfully prepared a TiO_2/Au/CdS Z-scheme photoanode and found out that its photo-electrochemical performance was hugely enhanced compared to TiO_2/CdS composite [23]. Naturally, metallic Ag would be introduced to construct an all-solid-state Z-scheme structure: $Ag_3PO_4/Ag/BiVO_4$, which could improve the transfer capability of photo-generated electron-hole pairs of $Ag_3PO_4/BiVO_4$ composite.

Furthermore, according to previous reports [24,25], a certain amount of heterojunction photocatalyst materials prepared by common chemical methods possessed the following problems: (I) the low proportion of structural elements with intimate interface and (II) the lattice mismatch between two semiconductors, further to lead to a decreased charge carriers separation efficiency. Functionalized graphene-based semiconductor photocatalyst could deal well with the above-mentioned issues to some extent, due to their high electron conductivity, large surface area and adsorption [26]. Graphene could serve as a good support to make the loaded nanoparticles to achieve uniform distribution without aggregation [27,28]. In addition, Wang and his co-workers validated that graphene played an important role in capturing and shuttling electrons in Ag_3VO_4/TiO_2/RGO composite, which resulted in an improved photo-induced electron-hole pairs separation efficiency [29]. As far as we know, relatively few studies were focused on building the all-solid-state Z-scheme photocatalyst based on $BiVO_4$ or Ag_3PO_4. Hence, Ag/Ag_3PO_4 nanoparticles and graphene were employed to construct graphene-bridged $Ag_3PO_4/Ag/BiVO_4$ Z-scheme heterojunction with superior photoactivity enhancement. Besides, the application for TC removal by this novel nanocomposite photocatalyst has not previously been reported.

Herein, the incorporation of Ag/Ag_3PO_4 nanoparticles and $BiVO_4$ onto graphene sheet was performed to obtain $Ag/Ag_3PO_4/BiVO_4$/RGO nanocomposite, which combined an in situ deposition with photo-reduction together. The co-catalytic effects between Ag/Ag_3PO_4 and RGO should contribute to the enhanced photocatalytic activity towards TC degradation under visible light irradiation. A series of operational conditions towards TC decomposition by $Ag/Ag_3PO_4/BiVO_4$/RGO nanocomposite were investigated in details, including catalytic behavior, catalysis dosage, initial TC concentrations, reaction pH, light irradiation condition, supporting electrolytes and water sources. It was worth noticing that the hierarchical assembly of graphene-bridged $Ag_3PO_4/Ag/BiVO_4$ Z-scheme heterojunction exhibited superior long-term photostability for TC degradation than those decompositions by pure $BiVO_4$ and Ag_3PO_4 nanocrystal. A possible photo-degradation mechanism was presented for better understanding the intrinsic reaction procedures by $Ag/Ag_3PO_4/BiVO_4$/RGO nanocomposite.

2. Experimental

2.1. Material and reagents

Bismuth nitrate pentahydrate ($Bi(NO_3)_3{\cdot}5H_2O$), ammonium metavanadate (NH_4VO_3), silver nitrate ($AgNO_3$), urea ($CO(NH_2)_2$), hydrazine hydrate ($N_2H_4{\cdot}H_2O$), disodium hydrogen phosphate (Na_2HPO_4), aqueous ammonia ($NH_3{\cdot}H_2O$), ethanol (CH_3CH_2OH), graphite powder and tetracycline (TC) were purchased from Ainopharm Chemical Reagent Co., Ltd. All chemicals were used without further purification. De-ionized water was used as the solvent throughout the experiment.

2.2. Synthesis of the catalysts

2.2.1. Preparation of $BiVO_4$

The monoclinic $BiVO_4$ sample with exposed (040) facets was fabricated by a homogeneous precipitation method according to previous reports [30,31]. Typically, 6 mmol of $Bi(NO_3)_3{\cdot}5H_2O$ was firstly dispersed into 32 mL of 1 M HNO_3 aqueous solution under ultrasonic treatment. Subsequently, NH_4VO_3 precursor (6 mmol) was added to the above clear suspension and kept vigorous stirring at room temperature for 1 h. After that, 3.0 g of urea was slowly added and the mixture was heated to 80 °C and maintained for 24 h under oil bath condition. A vivid yellow powder was separated by filtration, washed by ethanol and de-ionized water for several times, and finally dried at 60 °C overnight.

2.2.2. Preparation of RGO (1 wt%)/$BiVO_4$ nanocomposite

First of all, graphene oxide (GO) was prepared by a modified Hummer's method [32]. Then the as-prepared GO (0.012 g) was put into 50 mL de-ionized water and ultrasound treated for 1 h to disperse the samples thoroughly, followed by 1.2 g $BiVO_4$ was added into the GO dispersion and the mixture was ultrasounded for another 1 h. After 2 h stirring at room temperature, 1 mL $NH_3{\cdot}H_2O$ and 3 mL $N_2H_4{\cdot}H_2O$ was added drop by drop, the suspension was placed into a water bath at 80 °C for 4 h. After naturally cooling down, the precipitate was processed by filtration, rinsed with ethanol and de-ionized water for three times, respectively. The final product was dried at 60 °C for 12 h.

2.2.3. Preparation of Ag_3PO_4 (10 wt%)/$BiVO_4$ nanocomposite

The Ag_3PO_4 (10 wt%)/$BiVO_4$ composite were prepared by a facile in-situ deposition method. In detail, 0.5 g $BiVO_4$ was dispersed into 50 mL de-ionized water and the solution was sonicated for 30 min. Then 0.9 mmol of $AgNO_3$ was added quickly under violent stirring. After 30 min dark stirring, 20 mL Na_2HPO_4 solution (keep the molar ratio of Ag^+:PO_4^{3-} = 3:1) added dropwise to the above solution. When the mixture was violently stirred for 12 h in a dark condition, the precipitate was collected and washed it with de-ionized water and dried in a vacuum oven. For better comparison, pure Ag_3PO_4 photocatalyst was also prepared under the same condition without adding the as-synthesized $BiVO_4$ sample.

2.2.4. Preparation of $Ag/Ag_3PO_4/BiVO_4$/RGO nanocomposite

The $Ag/Ag_3PO_4/BiVO_4$/RGO composite was synthesized by a mild chemical and photo-deposition process. For fabricating the

above nanocomposite, $Ag_3PO_4/BiVO_4$/RGO was firstly constructed, followed by photo-reduction deposition of Ag nanoparticles onto the surface. Briefly, 0.25 g RGO/$BiVO_4$ was dispersed into 50 mL de-ionized water with ultrasonic processing until it became homogeneous. The $AgNO_3$ precursors (0.45 mmol) were added and kept stirring for 30 min at dark. After that, 0.15 mmol Na_2HPO_4 solution previously dissolved in 20 mL de-ionized water was added and the mixture maintained constant stirring for 12 h at room temperature. At last, the products were obtained by filtration, washing and drying. The previous-prepared $Ag_3PO_4/BiVO_4$/RGO (0.25 g) was added into 50 mL of methanol water solution with 10% volume concentration of concentration of methanol. Simultaneously, 0.0085 g $AgNO_3$ was added, and the dissolved mixture was irradiated by a 300 W Xe lamp for 60 min. Collected the precipitate and washed it with ethanol and de-ionized water for several times, and finally dried at 60 °C.

In addition, Ag (2 wt%)/$BiVO_4$ composite was also prepared by the same as-mentioned method above, where $BiVO_4$ was used to replace the role of $Ag_3PO_4/BiVO_4$/RGO in the $Ag_3PO_4/BiVO_4$/RGO nanocomposite.

2.3. Characterization

The crystallographic properties of the as-prepared samples were measured on a Rigaka D/max 2500v/pc X-ray diffractometer (Cu, Kα, λ = 0.154 nm, 40 kV, 40 mA) at a scan rate of 0.1° 2θ s^{-1}. Fourier transform infrared spectroscopy (FTIR) was collected on an IR Prestige-21 spectrometer (Shimadzu, Japan) at room temperature by the standard KBr disk method. Morphological analysis was performed by a field emission scanning electron microscope (FESEM, Hitachi S-4800) with 5.0 kV scanning voltages. The transmission electron microscopy (TEM) analysis of the samples was taken using a transmission electron microscope (TEM, FEI Tecnai G20) at an accelerating voltage of 200 kV). The UV–vis absorption spectra were recorded by n a UV–vis spectrometer (UV-4100, Shimadza) with an integrating sphere for the diffuse-reflectance spectroscopy (DRS), using $BaSO_4$ as the reference. The X-ray photoelectron spectroscopy (XPS) was carried out on a Thermo ESCALAB 250XI spectrometer with Al Kα source. The total organic carbon (TOC) assays were tested using a Shimadzu TOC-VCPH analyzer. Photoluminescence (PL) spectroscopy was monitored using a transient fluorescence spectrometer (Edinburgh FLsp920 full functional state). The Brunauer-Emmett-Teller (BET) surface area test was performed at 77 K on a TRISTAR-3000 surface area analyzer. The zeta potentials of the as-prepared samples were determined as a function of pH (adjusted by 0.1 M HNO_3 or NaOH) using a Zetasizer Nano-ZS (Malvern). The electron spin resonce (ESR) signals of radicals spin-trapped by spin-trapped reagent 5, 5-dimethyl-ʟ-pyrroline N-oxide (DMPO) and 2,2,6,6-Tetramethylpiperidinooxy (TEMPO) were examined on a Bruker ER200-SRC spectrometer under visible light irradiation (λ > 420 nm).

2.4. Photocatalytic experiments

The photocatalytic activity of graphene-modified $Ag_3PO_4/Ag/BiVO_4$ nanocomposite was evaluated by TC decomposition under visible light irradiation. A 300 W Xe lamp was employed as the light source with a 420 nm cut filter (light intensity: 100 mW cm^2). In each experiment, 50 mg photocatalyst was dispersed in an aqueous solution of TC (100 mL, 10 mg/L). Before the photocatalytic performances test, the suspension was stirred in the dark for 30 min to ensure the adsorption-desorption equilibrium between the catalyst and TC. During the illumination, an aliquot (3 mL) was sampled at certain time intervals, and then centrifuged at 10,000 rpm for 20 min and filtrated through a 0.22 μm Millipore filter to remove the residual particles. The corresponding concentration of TC was monitored by a Shimadzu UV–vis spectrophotometer with the absorbance at the characteristic band of 357 nm.

2.5. Photo-electrochemical measurements

The photocurrent was measured on CHI660B electrochemical workstation by using a standard three-electrode system. A platinum wire electrode, standard calomel electrode in saturated KCl and the as-prepared catalysts were used as the counter electrode, the reference electrode and working electrode, respectively. The working electrode was immersed in a sodium sulfate electrolyte solution (0.1 M) and illuminated under a visible light with the light intensity was 100 mW cm^2. Electrochemical impedance spectroscopy (EIS) was investigated on a potential Autolab PGSTAT-30 equipped with a frequency analyzer module using a three-electrode system in 0.1 M Na_2SO_4 solution. The electrochemical experimental results were all recorded with a CHI 660C electrochemical system. To prepare the working electrode, 10 mg photocatalyst was dispersed into 5 mL de-ionized water with ultrasonic treatment for 30 min. The suspension was then dip-coated for several times onto a 1 × 1 cm^2 fluorine-doped tin oxide glass electrode and for each time the conductive glass was dried at 60 °C for 30 min before next cycle.

3. Results and discussions

3.1. XRD analysis

XRD patterns providing information on the crystalline nature of a series of as-prepared samples were shown in Fig. 1. It could be observed that pure $BiVO_4$ powder was in good agreement with the body-centered monoclinic phase of $BiVO_4$ (JCPDS NO. 14-0688 [16,30]). The XRD pattern of Ag/$BiVO_4$ was similar to that of single $BiVO_4$, and no distinguishable characteristic peaks of Ag species detected, owing to the small dosage amount of metallic Ag in the composite [33]. Notably, no typical diffraction peaks belonging to separate graphene (RGO) were found in all graphene-modified $BiVO_4$ samples, which could be ascribed to the fact that the main characteristic peak of GO at around 12° was disappeared in the chemical reduction process [34]. The XRD results of $Ag_3PO_4/BiVO_4$, $Ag_3PO_4/BiVO_4$/RGO and Ag/$Ag_3PO_4/BiVO_4$/RGO curves revealed the peaks at 2θ of 29.6°, 33.4°, 36.5° and 55.0°, corresponding to (200), (210), (211) and (320) crystal planes of cubic Ag_3PO_4 (JCPDS file No. 06-0505 [18]). No additional crystal phases could be found in all patterns and presented with sharp diffraction peaks, implying no impurities generated in the fabrication procedure.

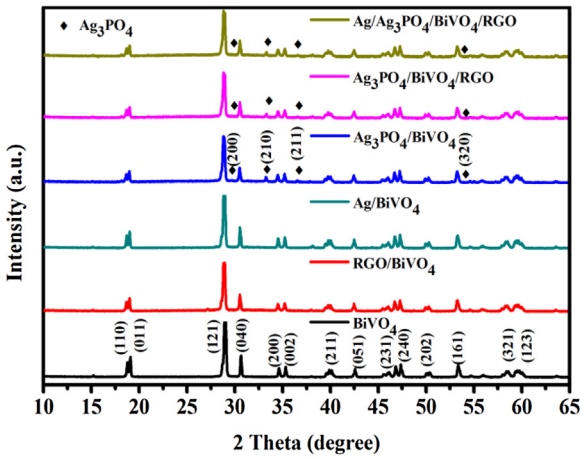

Fig. 1. XRD patterns of pure $BiVO_4$ and modified $BiVO_4$ samples.

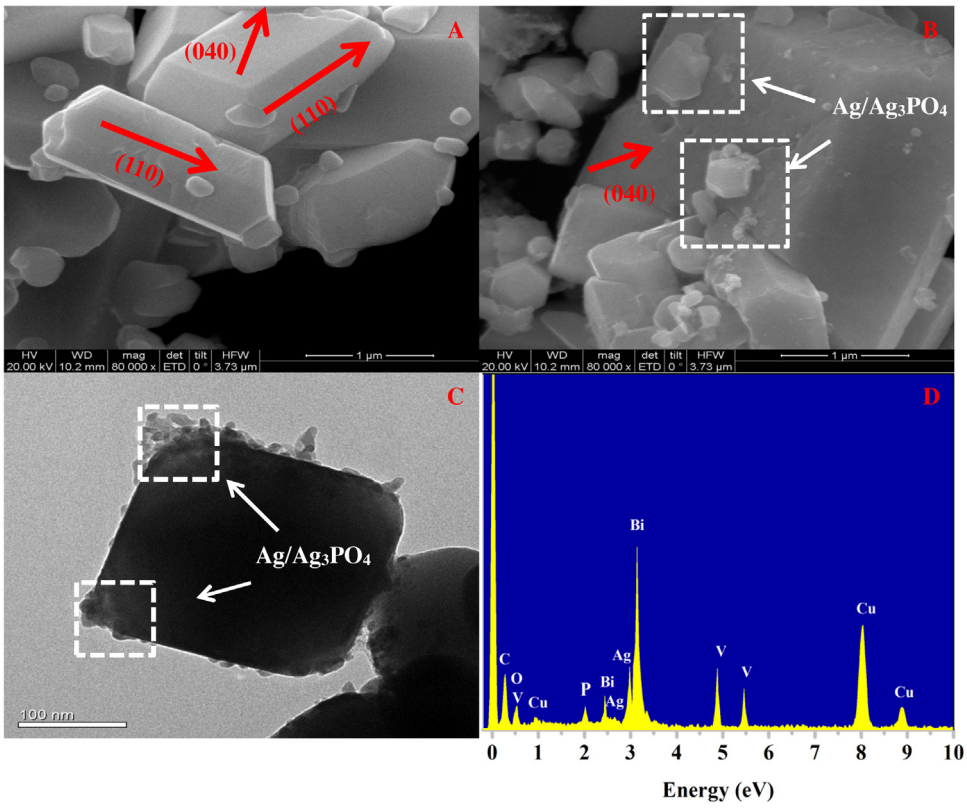

Fig. 2. SEM images of pure $BiVO_4$ (A) and $Ag/Ag_3PO_4/BiVO_4$/RGO (B); and TEM image (C) and EDS analysis (D) of $Ag/Ag_3PO_4/BiVO_4$/RGO.

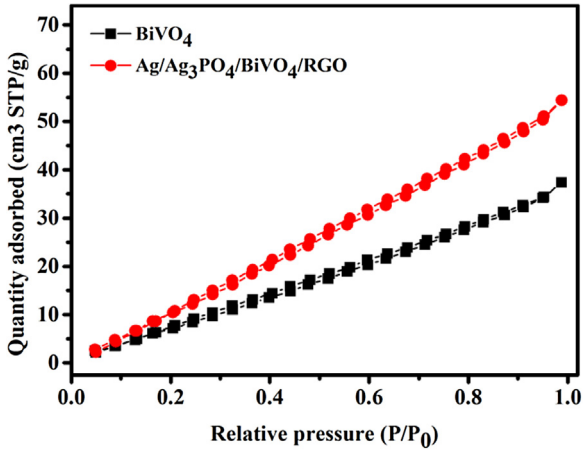

Fig. 3. Nitrogen adsorption-desorption isotherm of the as-prepared $BiVO_4$ and $Ag/Ag_3PO_4/BiVO_4$/RGO nanocomposite.

3.2. SEM, TEM and EDS analysis

To investigate the morphology and the detailed structure of the as-prepared samples, SEM images were detected as depicted in Fig. 2A-B. From Fig. 2A, it could be observed that the morphology of pure $BiVO_4$ samples displayed decagonal shape, where these well-defined crystals exhibited smooth surface and sharp edges with highly exposed facets. The two kinds of facets could be named as (040) and (110) [30], which played a significant role in charge carriers mobility. For $Ag/Ag_3PO_4/BiVO_4$/RGO nanocomposite (Fig. 2B), Ag/Ag_3PO_4 nanoparticles were found to be well deposited on the surface of $BiVO_4$ (040) crystal facet. Moreover, compared to pure $BiVO_4$, the surface of $Ag/Ag_3PO_4/BiVO_4$/RGO nanocomposite was rough to a certain extent, due to the attachment of graphene, which could enhance the surface area of reaction system and resulted in better photocatalytic performance [27,34]. The TEM technology (Fig. 2C) was further to confirm the emergence of Ag/Ag_3PO_4 nanoparticles on the surface of $BiVO_4$ with an unsmooth interface in the nanocomposite, which was well consistent with the SEM micrographs. Additionally, EDS spectrum was also adopted to analyze the elements in $Ag/Ag_3PO_4/BiVO_4$/RGO nanocomposite and the result was shown in Fig. 2D. The essential elements of Bi, V, Ag, P, O and C were observed and the weight ratio of $Ag_3PO_4/BiVO_4$ was about 9.69%, in good accordance with the preparation proportion (10 wt%). Furthermore, the stoichiometric proportion of Ag to P was about 3.2:1, which was a little higher the theoretical molar ratio of 3:1 for Ag_3PO_4 composite. This phenomenon could be ascribed to the production of metallic Ag in the photo-reduction process. The above-mentioned information confirmed the co-existence of Ag/Ag_3PO_4 nanoparticles and RGO in the nanocomposites.

3.3. BET and XPS analysis

Fig. 3 illustrated the N_2 adsorption-desorption isotherms of pure $BiVO_4$ and $Ag/Ag_3PO_4/BiVO_4$/RGO nanocomposite. Both of the samples possessed a type II isotherm and a type H_3 hysteresis loop in the relative pressure range of 0.9–1.0, indicative of macropore pressure. Compared to pure $BiVO_4$ (surface area = 29.63 m^2/g, pore size = 14.43 nm, total pore volume = 0.069 cm^3/g, Table 1), $Ag/Ag_3PO_4/BiVO_4$/RGO nanocomposite displayed a higher surface area (57.58 m^2/g), pore size (14.74 nm) and total pore volume (0.103 cm^3/g), suggesting that the synthetic effects of Ag/Ag_3PO_4 nanoparticles and RGO facilitated the enhanced reaction area, which was in good accordance with the adsorption results in darkness.

Surface chemical states of pure $BiVO_4$ and $Ag/Ag_3PO_4/BiVO_4$/RGO nanocomposite were studied by the means of the XPS

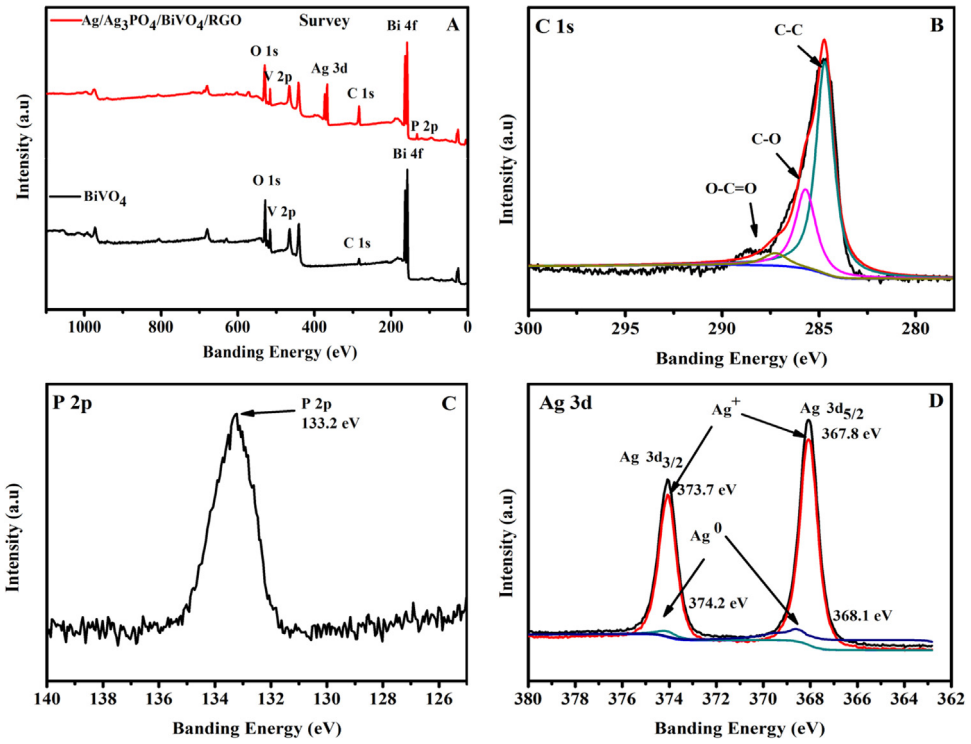

Fig. 4. XPS spectrum of the pure $BiVO_4$ and $Ag/Ag_3PO_4/BiVO_4/RGO$: (A) survey spectrum; (B) C 1s; (C) P 2p and (D) Ag 3d.

Table 1
Surface area, pore size and pore volume parameters for pure $BiVO_4$ and $Ag/Ag_3PO_4/BiVO_4/RGO$ nanocomposite.

Samples	Surface area[a] (m^2/g)	Pore size[b] (nm)	V_t[c] (cm^3/g)
$BiVO_4$	29.63	14.43	0.069
$Ag/Ag_3PO_4/BiVO_4/RGO$	57.58	14.74	0.103

[a] Measured using N_2 adsorption with the Brunauer-Emmett-Teller (BET) method.
[b] Pore size in diameter calculated by the desorption data using Barrett-Joyner-Halenda (BJH) method.
[c] Total pore volume determined at $P/P_0 = 0.99$.

technique. The survey spectrum in Fig. 4A, indicated that the elements Bi, V, Ag, P, O and C existed in the $Ag/Ag_3PO_4/BiVO_4/RGO$ nanocomposite while only the peaks of Bi, V, O and C appeared in pure $BiVO_4$. XPS spectra were obtained to prove the reduction of GO to RGO by detecting the chemical state of C species in the nanocomposite. Fig. 4B displayed the C 1 s spectra of $Ag/Ag_3PO_4/BiVO_4/RGO$ could be decomposed into three characteristic peaks, which were attributed to the following functional groups: sp^2 bounded carbon (C—C, 284.5 eV), epoxy/hydroxyls (C—O, 286.8 eV) and carboxyl (O—C=O, 288.8 eV [34,35]). The binding energy peak at 133.2 eV could be ascribed to the electron orbit of P 2p (Fig. 4C). As shown in Fig. 4D, two characteristic peaks located at 373.7 eV and 367.8 eV could be assigned to the electron orbits of Ag $3d_{3/2}$ and Ag $3d_{5/2}$, respectively. After decomposing the above two binding energy peaks in curve fitting processing, it could be observed that the strong binding energy peaks at 373.7 eV and 367.8 eV, corresponded to Ag^+, while another two weak peaks at 374.2 eV and 368.1 eV owing to the presence of Ag^0 [30,36]. The results indicated that metallic Ag was successfully introduced under the photoreduction procedure.

3.4. Photocatalytic degradation of TC

The photocatalytic capability of the $Ag/Ag_3PO_4/BiVO_4/RGO$ composites was investigated by the decomposition of tetracycline under various conditions including catalytic behavior, catalysis dosage, initial TC concentrations, reaction pH, light irradiation condition, supporting electrolytes and water sources. Taken the practical application into consideration, the photo-stability and mineralization ability of the as-prepared samples were also evaluated.

3.4.1. Effect of catalytic behavior

Fig. 5A displayed results of the effect of catalytic behavior on the decomposition of TC as a function of irradiation time. The concentration of TC decreased gradually as the exposure time increased for all samples. It could be observed that the as-prepared photocatalysts showed different degradation rates for TC removal, which was in the order of $Ag/Ag_3PO_4/BiVO_4/RGO > Ag_3PO_4/BiVO_4/RGO > Ag_3PO_4/BiVO_4 > RGO/BiVO_4 > Ag/BiVO_4 > BiVO_4$. The pure $BiVO_4$ exhibited the lowest TC removal efficiency of only ca. 56.33% within 60 min visible light irradiation, while $Ag/Ag_3PO_4/BiVO_4/RGO$ nanocomposite possessed the highest removal efficiency (ca. 94.96%) under the identical condition. Combining with absorption ability analysis in Fig. 5B, the adsorption-desorption equilibrium between TC and the catalyst was acquired within 30 min dark reaction. Moreover, the successful introduction of Ag/Ag_3PO_4 and RGO in the constructed heterojunction was also good for the adsorption ability enhancement. The above-mentioned results demonstrated that modified $BiVO_4$ exhibited obviously adsorption abilities and photocatalytic activities. Among these prepared photocatalysts, $Ag/Ag_3PO_4/BiVO_4/RGO$ nanocomposite obtained the optimum photocatalytic performance, which could be ascribed to the enhanced adsorption activity of the composite photocatalyst for TC and the high migration efficiency of photo-induced electron-hole pairs. Therefore, in the graphene-modified $Ag_3PO_4/Ag/BiVO_4$ heterojunction, the co-catalyst effect between Ag/Ag_3PO_4 and RGO on the surface of $BiVO_4$ played an important role in suppressing the electron-hole recombination in the photocatalytic system.

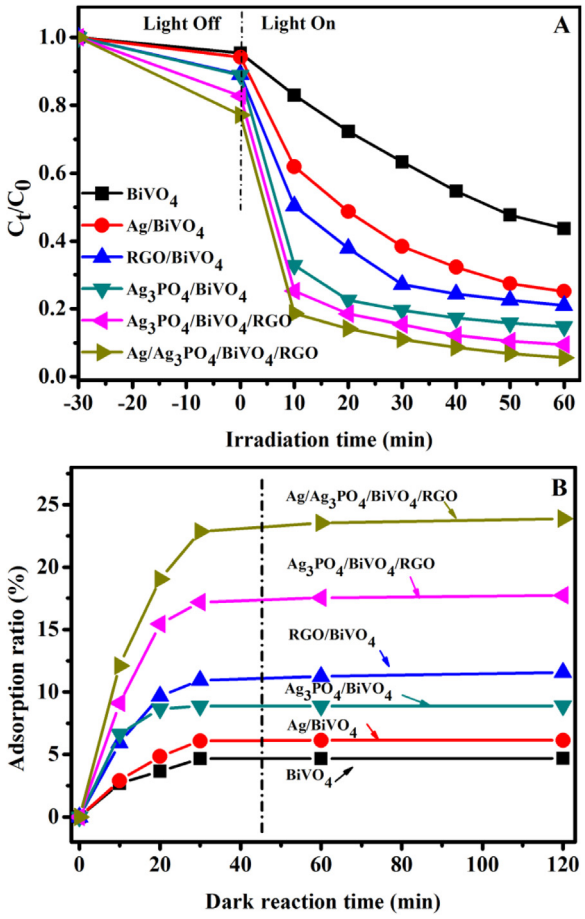

Fig. 5. (A) Photocatalytic degradation of TC in the presence of different photocatalysts under visible light irradiation; (B) Absorption ability evaluation of the as-prepared samples for TC removal in dark condition (Experimental conditions: initial TC concentration = 10 mg/L, pH = 6.75, m = 50 mg, V = 100 mL, visible light: λ > 420 nm).

3.4.2. Effect of catalysis dosage

Considering the practical applications in the industrial production, lowering the cost as much as possible played an important role in experimental investigations [37]. The experiments were performed to observe the decomposition of TC with different catalyst dosage in the range of 0.10–2.00 g/L. As depicted in Fig. 6A, when the catalyst dosage increased from 0.10–0.50 g/L, the corresponding degradation efficiencies of TC increased from 65.39% to 95.67%. Nevertheless, when higher dosage (0.50–2.00 g/L) of $Ag/Ag_3PO_4/BiVO_4/RGO$ catalyst was added into the reaction system, the resulting degradation efficiencies decreased to a greater level along with the increasing catalyst amount. The information suggested that moderate dosage of photocatalyst was necessary to achieve superior photocatalytic properties, further to verify the previous research founding that on one hand, higher catalyst dosage could lead to more production of active species in the photocatalytic procedure and on the other hand, excess catalyst dosage accumulated turbidity of the solution and reduction of the light penetration through the TC solution in return [38,39]. Herein, the catalyst dosage located at ca. 0.50 g/L was picked out as the best for the following investigations.

3.4.3. Effect of initial TC concentrations

Fig. 6B showed the TC degradation with different initial concentrations using $Ag/Ag_3PO_4/BiVO_4/RGO$ nanocomposite. It could be detected that the initial TC concentration had a great impact on the whole photo-degradation process, where 94.96%, 82.89%, 70.30%, 53.69% and 45.57% of TC were removed at the initial TC concentration equal to 10, 20, 30, 40 and 50 mg/L, respectively. Higher initial pollutant concentrations could possess negative effect in the photocatalytic reaction, which could lead to the decrease of the path length of the photon entering the TC solution. As a result, less photons could transfer to the catalyst surface due to the reduced light penetration at high initial concentration, which was similar to the previous reports [38,40]. Besides, intermediates could compete with the TC compound for the limited adsorption and catalytic sites on the catalyst surface adsorption [41]. Competition between TC molecules and intermediates was enhanced along with the increasing TC concentration, due to the more production of intermediates at high pollutant concentration. Furthermore, high TC removal at low concentrations was considered to be of a great importance [10]. Thus, the initial TC concentration was chosen as 10 mg/L in the whole experiments.

3.4.4. Effect of reaction pH

The initial pH of the aqueous solution might influence the generation of ROSs and have a great effect on photocatalytic reaction [42]. As shown in Fig. 6C, a series of pH values were controlled by NaOH (0.1 M) or HNO_3 (0.1 M) to explore the effect of initial pH in the photocatalytic process. Table 2 listed out the corresponding Zeta potentials of $Ag/Ag_3PO_4/BiVO_4/RGO$ composite before or after visible light reaction as a function of solution pH, $Ag/Ag_3PO_4/BiVO_4/RGO$ composite had an overall negative surface charge at pH 3–11. A more negative potential was tested along with the increasing pH values. Electrostatic attraction might play an important role in the adsorption ability, which could be enhanced between the opposite positively charged TC molecules and negatively charged $Ag/Ag_3PO_4/BiVO_4/RGO$ nanocomposite. Although strong adsorption of the TC took place at high pH, excessive TC adsorption might block light from arriving at the catalyst surface, reduce the surface light intensity, and impeded the hole-electron photoexcitation process subsequently. In addition, the negatively charged photocatalyst surface prevented the sorption of hydroxide ions, resulting in the decrease of hydroxyl radicals forming and photocatalytic activity. In this study, the optimum pH value was set at ca. 6.75 owing to the obtained highest photoactivity.

3.4.5. Effect of light irradiation condition

Sunlight would be one of the best choices in future energy source because of its easy accessibility and perferable abundance. As depicted in Fig. 6D, photocatalytic degradation of TC was studied with and without the optical filter being placed in front of the 300 W Xe lamp. It could be found that there was no significant loss in TC concentration in the 60 min irradiation (catalyst dosage: 0.50 g/L, initial concentration: 10 mg/L) beside the adsorption amount in dark condition. Without the optical filter, the $Ag/Ag_3PO_4/BiVO_4/RGO$ nanocomposite was exposed to the full spectrum of the 300 W Xe lamp. Compared with photocatalytic procedure with the filter (λ > 420 nm), a greater removal efficiency could be obtained under full spectrum condition, where the degradation efficiency could reach to 96.21% only in first 10 min exposure time. Similar phenomenon was also observed both with and without the catalyst, even though the removal efficiency without photocatalysts could be ignored (with filter: 1.39%; without filter: 5.46%). The shorter the wavelength of the light used, the greater photons energy would be achieved, resulting in the increasing photocatalytic performance under the identical condition. The result validated that the valuable application potential of $Ag/Ag_3PO_4/BiVO_4/RGO$ photocatalyst in practical wastewater treatment, owing to the full wavelength for the natural sunlight.

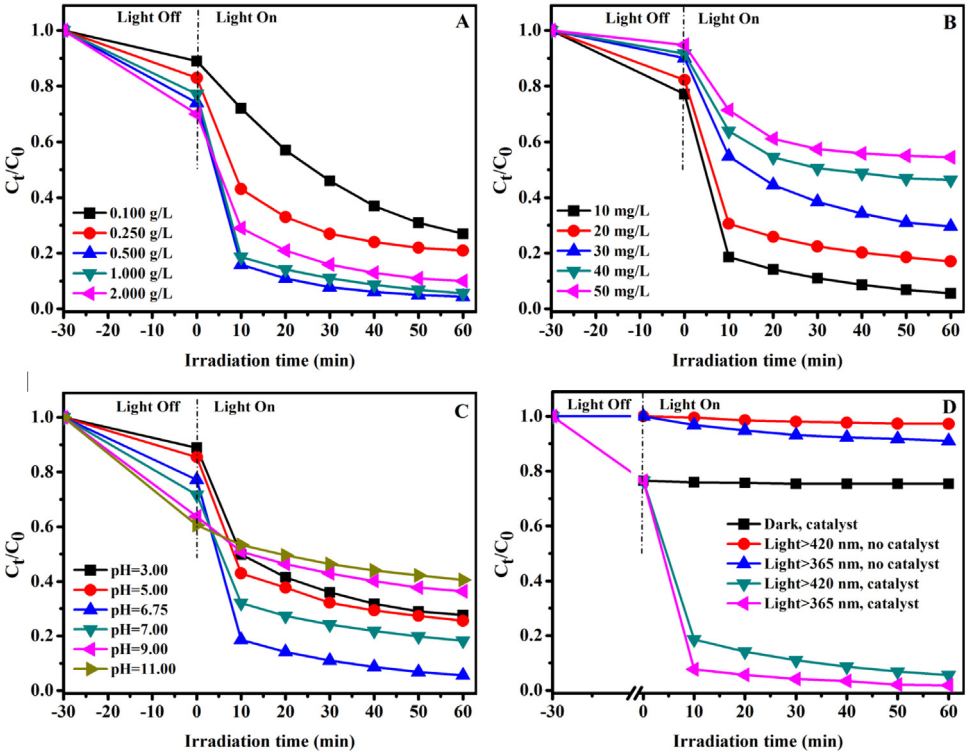

Fig. 6. Effects of (A) catalysis dosage; (B) initial TC concentrations; (C) initial pH and light irradiation condition (D) on the degradation of TC over $Ag/Ag_3PO_4/BiVO_4/RGO$ nanocomposite under visible light irradiation.

Table 2
The Zeta potentials of $Ag/Ag_3PO_4/BiVO_4/RGO$ composite before or after visible light reaction as a function of solution pH.

pH	3	5	6.75	7	9	11
ξ-potential[a]	−3.03 ± 0.28	−10.16 ± 2.13	−26.52 ± 1.07	−31.73 + 3.01	−42.05 ± 1.89	−49.31 ± 0.98
ξ-potential[b]	−4.18 ± 0.21	−20.08 ± 2.35	−22.64 ± 1.78	−29.23 ± 1.90	−37.09 ± 3.32	−49.54 ± 0.54

I. [a] and [b] represent the ξ-potentials (mV) of $Ag/Ag_3PO_4/BiVO_4/RGO$ composite before or after visible light reaction, respectively.
II. Experimental conditions: m/V = 0.50 g/L, TC (100 mL, 10 mg/L), visible light (λ > 420 nm).

3.4.6. *Effect of supporting electrolytes*

It is well-known that chlorine, sulfate and bicarbonate ions are the most common anions in natural water and most of them existed as the form of salts. Furthermore, supporting electrolyte could interface with the photocatalytic reaction in practical wastewater application. Herein, NaCl, Na_2SO_4 and Na_2CO_3 were adopted to investigate the detail effects on the photocatalytic degradation of TC by $Ag/Ag_3PO_4/BiVO_4/RGO$ nanocomposite. Fig. 7A displayed the results of TC removal in the presence of the above electrolytes at a concentration of 0.05 M, the corresponding decreasing order as follows: Na_2SO_4 > NaCl > Na_2CO_3. A slight promotion could be found within the Na_2SO_4 electrolyte, but the difference was insignificant. Unlike the effect of Na_2SO_4, the negative effects were found in the presence of NaCl and Na_2CO_3. The decrease in the photodegradation of TC might be ascribed to the competitive adsorption between Cl^- and TC on the surface of the catalyst. According to previous reports, bicarbonate and carbonate ions were the radical scavengers [43]. For example, Zhou et al. found that the hydroxyl radicals generated at the surface of Co-doped $BiVO_4$ might be captured with the addition of carbonate ions [41]. The presence of carbonate ions would contribute to the decreasing photocatalytic activity. Meanwhile, the Zeta potentials (ξ-potentials) of $Ag/Ag_3PO_4/BiVO_4/RGO$ composite in the presence of different supporting electrolytes were also listed in Table 3, which could be put in the following order; NaCl > Na_2SO_4 > Na_2CO_3. The ξ-potentials before (−23.92 ± 0.18 mV) or after (−21.90 ± 0.27 mV) reactions with the supporting electrolyte of Na_2SO_4 were closer to those (before: −26.52 ± 1.07 mV; after: −22.64 ± 1.78 mV) of the condition at pH = 6.75, further to testify the negative effect with the lower ξ-potentials. The competitive adsorption between TC molecules and Na^+ on the adsorption sites of $Ag/Ag_3PO_4/BiVO_4/RGO$ might also lead to the lower photocatalytic activity.

Table 3
Zeta potentials (ξ-potentials) of $Ag/Ag_3PO_4/BiVO_4/RGO$ composite in the presence of different supporting electrolytes.

Supporting Electrolyte	NaCl	Na_2SO_4	Na_2CO_3
I. ξ-potential (mV)	−15.94 ± 0.43	−23.92 ± 0.18	−30.63 ± 2.35
II. ξ-potential (mV)	−16.89 ± 1.09	−21.90 ± 0.27	−32.96 ± 1.78

a. I and II represent the procedure of before and after irradiation.
b. Experimental conditions: m/V = 0.50 g/L, TC (100 mL, 10 mg/L), pH = 6.75, visible light (λ > 420 nm) and the concentration of supporting electrolyte: 0.5 mol/L.

3.4.7. *Effect of water sources*

The initial water status might also an important parameter in the real wastewater application. The effect of various wastewaters for the removal of TC using $Ag/Ag_3PO_4/BiVO_4/RGO$ nanocomposites was shown in Fig. 7B. After the adsorption and photocatalytic reactions, degradation efficiencies were more than 94.96%. 84.21%, 83.43%, 80.21% and 87.23% were achieved in TC-obtained deionized water, medical wastewater, municipal wastewater, river wastewater and tap wastewater, respectively. Certainly, reduction

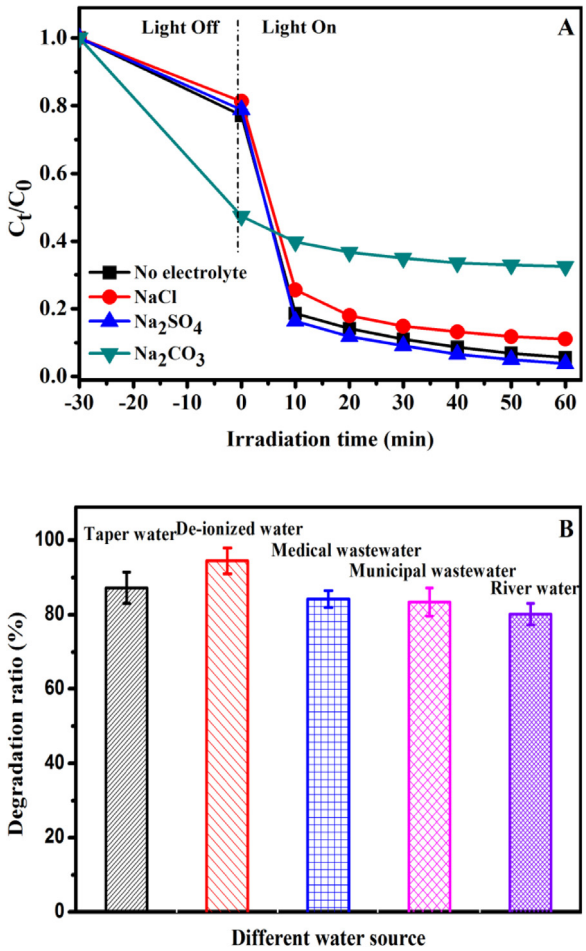

Fig. 7. Effect of supporting electrolyte (A) and water sources (B) on the degradation of TC over $Ag/Ag_3PO_4/BiVO_4/RGO$ nanocomposite under visible light irradiation.

efficiencies in different degrees were investigated in different water sources due to the existing competitive pollutants, but relatively high removal ratios were all obtained. Hence, it could be inferred that $Ag/Ag_3PO_4/BiVO_4/RGO$ nanocomposite possessed a long-term application potential for wastewater purification.

3.4.8. *Photocatalyst recyclability and mineralization ability tests*

The chemical stability and reusability of the photocatalysts were very important for practical applications. Consequently, the photocatalytic stability of pure $BiVO_4$, pure Ag_3PO_4 and $Ag/Ag_3PO_4/BiVO_4/RGO$ were investigated relative to TC degradation by repeating the reaction for four times. For each cycle, the catalyst was collected by filtration, washing and drying before next run. As shown in Fig. 8A–C, the degradation efficiency of $Ag/Ag_3PO_4/BiVO_4/RGO$ after four times recycling was rather stable and remained about 93.28% (only about 1.68% loss, Fig. 8A), which was much higher than those of pure $BiVO_4$ (46.69%, Fig. 8B) and pure Ag_3PO_4 (49.89%, Fig. 8C). For pure $BiVO_4$, a loss of about 10.22% in the degradation efficiency was observed. Pure Ag_3PO_4 exhibited an obvious decrease in the removal efficiency in four successive experimental runs under the same conditions and about 22.23% of photo-degradation efficiency was lost at the fourth cycle. Moreover, the samples of before or after photocatalytic reaction were characterized by XRD analysis (Fig. 8D), it could be found that the XRD pattern of the recycled $Ag/Ag_3PO_4/BiVO_4/RGO$ nanocomposite had almost no obvious discrepancy compared with the unirradiated one. The results demonstrated the combination of Ag/Ag_3PO_4 and RGO could significantly increase not only the photocatalytic degradation performance but also the photocatalytic degradation stability of pure $BiVO_4$ and Ag_3PO_4.

Fig. 9 presented that the total organic carbon (TOC) removal by the as-prepared samples. After 60 min irradiation, a mineralization rate of 7.89% and 27.42% for pure $BiVO_4$ and $Ag/Ag_3PO_4/BiVO_4/RGO$ nanocomposite, suggesting higher mineralization ability was achieved by the modified $BiVO_4$.

3.5. *Light absorption and charge transfer properties*

UV/vis diffuse reflectance spectrum was measured to characterize the optical bandgap and absorption capability of the as-prepared photocatalysts. As shown in Fig. 10A, the absorption edge of pure $BiVO_4$ is about 516 nm, originated from its band gap of about 2.4 eV, in good accordance with reported results [17]. It could be observed that an obvious enhancement in the visible light absorptions of modified $BiVO_4$. In all the samples, $Ag/Ag_3PO_4/BiVO_4/RGO$ nanocomposite possessed the mostly widely spectral response in visible light wavelength. The results inferred that the fabricated graphene-bridged $Ag_3PO_4/Ag/BiVO_4$ Z-scheme heterojunction could greatly improve the optical absorption due to co-catalytic effects between Ag/Ag_3PO_4 nanoparticles and RGO, which is beneficial to generate more electron-hole pairs and then lead to the greater photocatalytic efficiencies towards pollutants degradation.

Photoluminescence (PL) spectra has been performed to reveal the charge carrier trapping, migration and recombination processes of the semiconductor photocatalysts since PL emission arises from the recombination of free carriers [32]. Fig. 10B

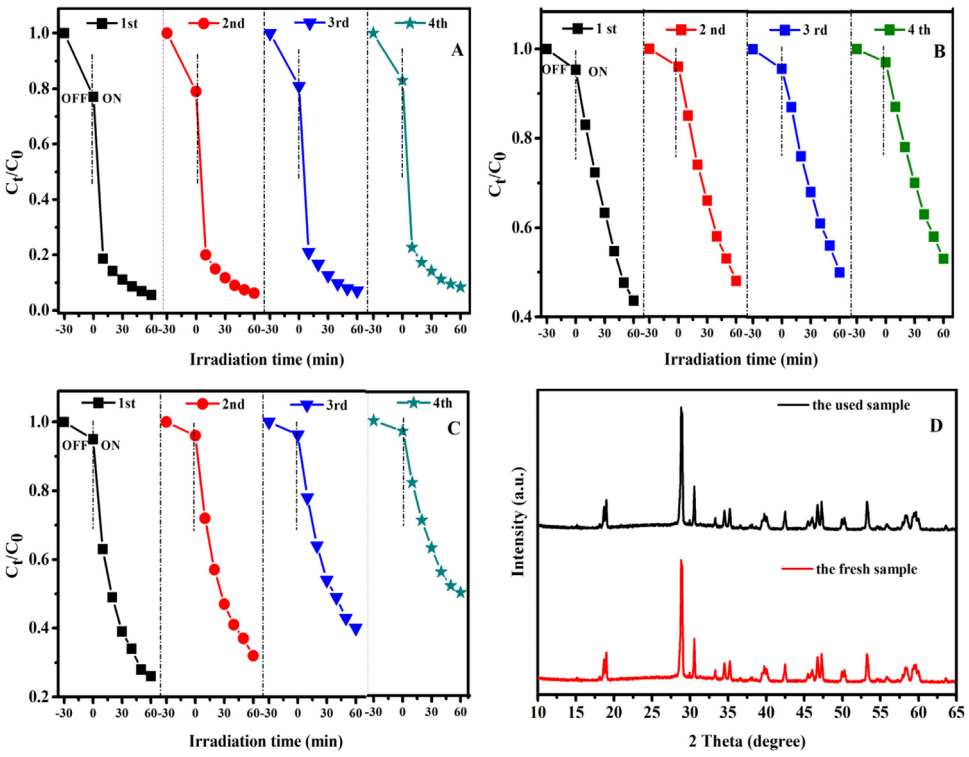

Fig. 8. Cycling performances of photocatalytic degradation of TC over (A) $Ag/Ag_3PO_4/BiVO_4$/RGO, (B) pure $BiVO_4$ and (C) pure Ag_3PO_4 (Experimental conditions: initial TC concentration = 10 mg/L, pH = 6.75, m/V = 0.50 g/L, visible light: λ > 420 nm); and (D) XRD patterns of the fresh and used $Ag/Ag_3PO_4/BiVO_4$/RGO nanocomposite.

showed the PL spectra of the pure $BiVO_4$, $Ag/BiVO_4$, $RGO/BiVO_4$, $Ag_3PO_4/BiVO_4$, $Ag_3PO_4/BiVO_4$/RGO and $Ag/Ag_3PO_4/BiVO_4$/RGO nanocomposites. Upon the excitation wavelength at 420 nm, the main emission peak of $BiVO_4$ was detected at around 521 nm, owing to the band gap recombination of electron-hole pairs. [44] Pure $BiVO_4$ possessed a relatively high recombination rate of photo-induced carriers, which was decreased in the presence of Ag nanoparticles, RGO and Ag_3PO_4. As presented in Fig. 10B, the PL intensities of the as-prepared samples were ranked as: $BiVO_4$ > $Ag/BiVO_4$ > $RGO/BiVO_4$ > $Ag_3PO_4/BiVO_4$ > $Ag_3PO_4/BiVO_4$/RGO > $Ag/Ag_3PO_4/BiVO_4$/RGO, which was in good accordance with the result of photocatalytic behaviors. Generally speaking, lower the PL signal means that the higher separation efficiency of electron-hole pairs. It was clearly observed that $Ag/Ag_3PO_4/BiVO_4$/RGO nanocomposite had the lowest peak intensity than other samples, implying that the cooperative effects between RGO and Ag/Ag_3PO_4 contributed to decreasing the recombination of electron-hole pairs effectively and enhancing the charge separation efficiency.

The charge separation and migration could significantly affect the photocatalytic performance, which could be verified by the photocurrent response. In this study, photocurrent densities vs time curve was conducted to the same electrolyte with several 20 s light on/off at 0 V vs Ag/AgCl. As displayed in Fig. 10C, a clear comparison of the I-t curves for the as-prepared photocatalysts under visible light irradiation (λ > 420 nm). For pure $BiVO_4$, modified $BiVO_4$ showed the higher photocurrent intensity. Especially, $Ag/Ag_3PO_4/BiVO_4$/RGO nanocomposite could achieve a photocurrent of $1.88 \pm 0.09\ mA\ cm^{-2}$, which was much higher than the photocurrents of $BiVO_4$ ($0.56 \pm 0.06\ mA\ cm^{-2}$), $RGO/BiVO_4$ ($0.92 \pm 0.07\ mA\ cm^{-2}$) and $Ag_3PO_4/BiVO_4$ ($1.42 \pm 0.05\ mA\ cm^{-2}$). The result demonstrated that the interaction existed in $Ag/Ag_3PO_4/BiVO_4$/RGO rather than simple mixture. The highest photocurrent obtained by $Ag/Ag_3PO_4/BiVO_4$/RGO could be ascribed to the efficient electron-hole transfer and separation process, which was beneficial from the co-effect of both RGO and Ag/Ag_3PO_4 nanoparticles. The introduction of Ag/Ag_3PO_4 nanoparticles played an important role in charge separation, and the emergence of RGO could collect more photo-electrons and commendably shuttle electrons through the Π–Π network [24,29].

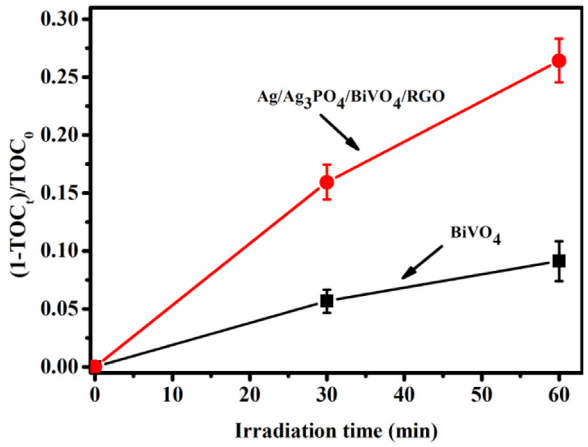

Fig. 9. TOC removal in the prsence of pure $BiVO_4$ and $Ag/Ag_3PO_4/BiVO_4$/RGO nanocomposite under visible light irradiation.

Moreover, electrochemical impedance spectra (EIS) test was also an effective way to analyze the separation and transfer of electron/hole pairs. The semicircle in the Nyquist plots in EIS measurements provides information on the charge process with the diameter of the semicircle corresponding to the charge transfer resistance, where a smaller arc radius indicates higher efficiency in charge transfer [30]. Fig. 10D showed the Nyquist plots of pure $BiVO_4$ and modified $BiVO_4$ electrodes under visible light conditions. Among those prepared samples, $Ag/Ag_3PO_4/BiVO_4$/RGO under vis-

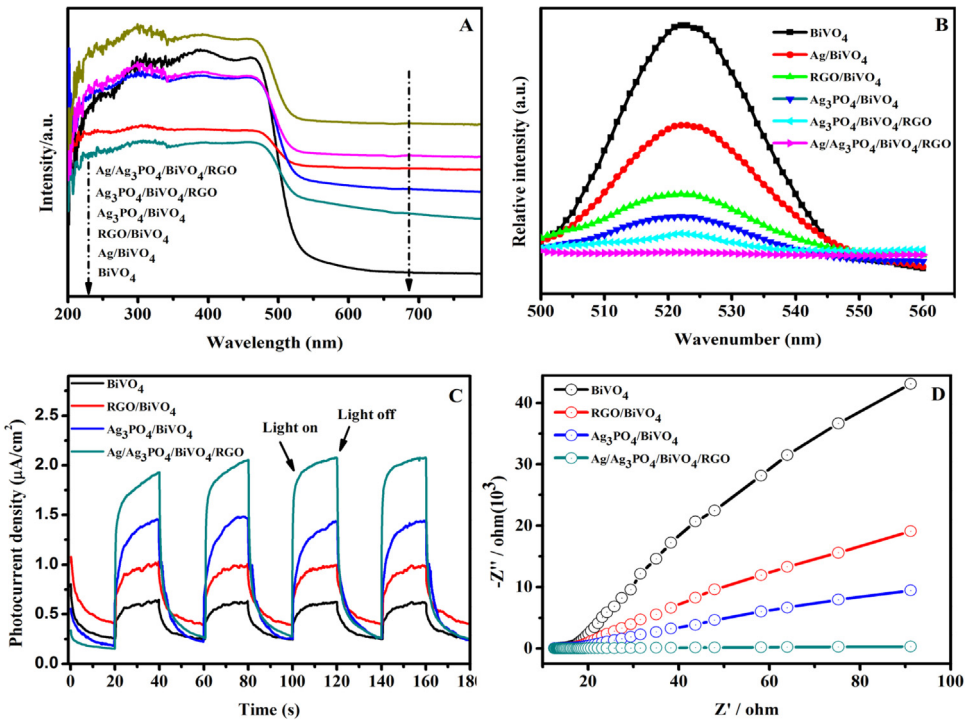

Fig. 10. (A) UV–vis absorption (DRS) spectra; (B) Photoluminescene (PL) spectra; (C) Photocurrent (PC) responses and (D) Electrochemical impedance spectroscopy (EIS) analysis of the as-prepared samples: pure $BiVO_4$ and modified $BiVO_4$.

ible light irradiation possessed the smallest semicircular diameter, suggesting the fastest separation and transfer of photo-generate carriers over $Ag/Ag_3PO_4/BiVO_4/RGO$ nanocomposite. The above point was well consistent with the results of photocatalytic activity.

3.6. Possible photocatalytic mechanism in reaction system

The presence of graphene and Ag/Ag_3PO_4 nanoparticles in the $Ag/Ag_3PO_4/BiVO_4/RGO$ nanocomposite could effectively inhibit the electron-hole pair recombination, which might cause more radical species with strong oxidation capability. To explore the predominant active species generated in the reaction system, three typical chemicals, 1,4-benzoquinone (BQ), Ethylenediamintetraacetic acid disodium (EDTA-2Na) and Isopropanol (IPA) were employed as the scavengers of superoxide radical ($^{\bullet}O_2^-$ [38]), hole (h^+ [10]) and hydroxyl radical ($^{\bullet}OH$ [45]), respectively. As depicted in Fig. 11, when 1 mmol of IPA as the scavenger for $^{\bullet}OH$ radical species was added into the photocatalytic procedure, the degradation efficiency of TC was slightly depressed, indicating that few $^{\bullet}OH$ was involved in the TC photodegradation. The degradation efficiency of TC obviously decreased from 94.96% to 30.34% in the presence of 1 mmol EDTA-2Na, suggesting the active species of holes played an important role towards TC degradation. Similarly, a significant loss (percentage of degradation ratio reduction) could be found with the addition of 1 mmol of BQ, verifying the $^{\bullet}O_2^-$ pathway possessed a crucial role in the TC oxidation. To further confirm the point, a N_2 purging experiment was also carried out, the removal efficiency of TC was hugely hampered by the conducted N_2 (no scavenger), which decreased from initial removal efficiency 94.96% under air-equilibrated conditions to 48.78% under N_2 atmosphere. The result demonstrated that the dissolved oxygen which could act as a photo-generated electron scavenger to produce $^{\bullet}O_2^-$ radical species. As a result, it could be preliminarily concluded that h^+ and $^{\bullet}O_2^-$ generated in the photocacalytic system should be responsible for the enhanced photo-oxidation performance towards TC decomposition.

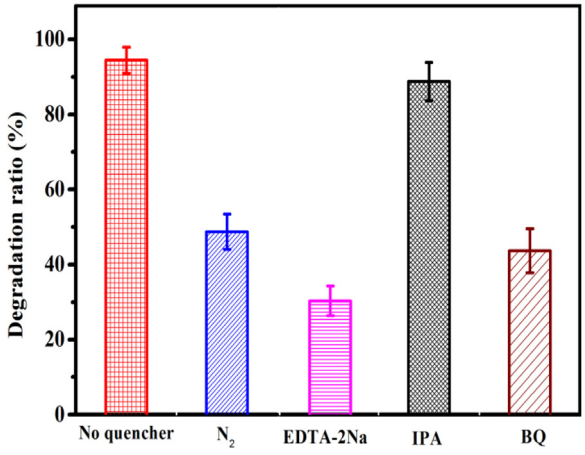

Fig. 11. Trapping experiment of active species during the photocatalytic degradation of TC over $Ag/Ag_3PO_4/BiVO_4/RGO$ nanocomposite under visible light irradiation.

In order to further confirm the above-obtained radical generation in this photocatalytic system under visible irradiation, the ESR spin-trap with DMPO and TEMPO techniques were performed on illuminated $Ag/Ag_3PO_4/BiVO_4/RGO$ nanocomposite. All the experiments were operated under dark condition and visible light irradiation of 4 min, 8 min and 12 min. As shown in Fig. 12A, four characteristic peaks of DMPO-$^{\bullet}O_2^-$ were observed in methanol dispersion under visible light irradiation. Notably, stronger intensity DMPO-$^{\bullet}O_2^-$ adducts were found under visible light irradiation, while no signals in dark condition, indicating that $^{\bullet}O_2^-$ played an important role in the degradation system. From Fig. 12B, no obvious signals of $^{\bullet}OH$ were detected in the system containing $Ag/Ag_3PO_4/BiVO_4/RGO$ in the aqueous dispersion under visible light irradiation, which suggested that $^{\bullet}OH$ oxidation was not the predominant reaction species during the photocatalytic process. Moreover, photo-induced holes (h^+) were also tested. The signal

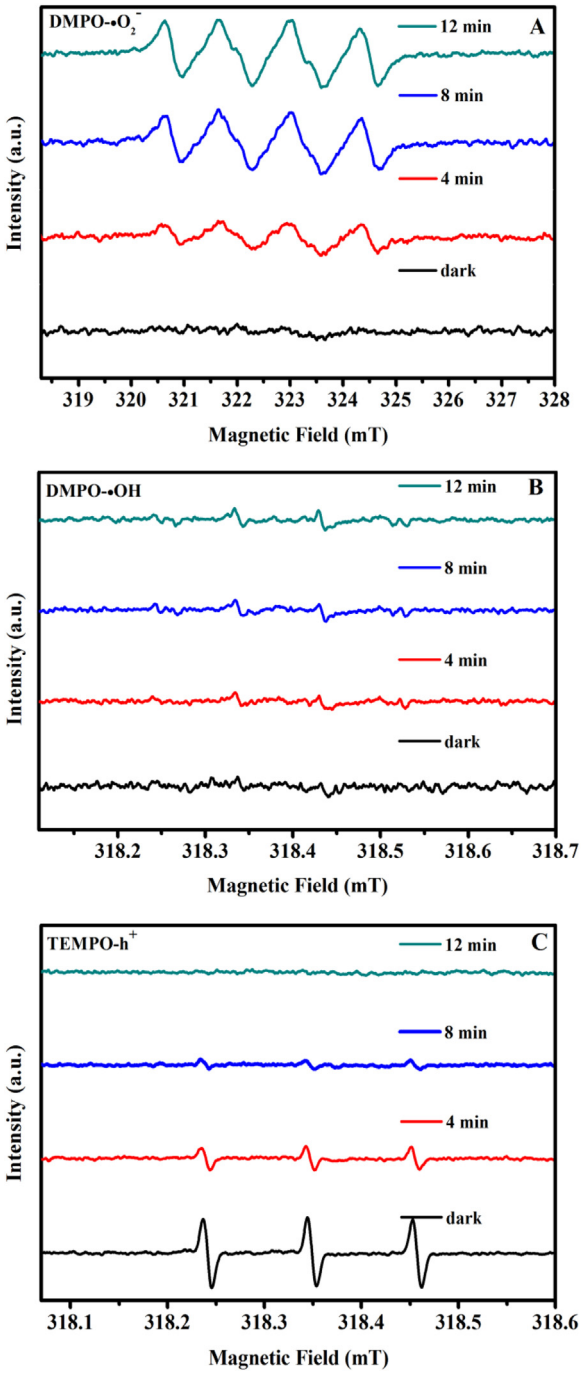

Fig. 12. ESR spectra of radical adducts trapped by DMPO ($^{\bullet}O_2^-$ and $^{\bullet}OH$) and TEMPO (h^+) in $Ag/Ag_3PO_4/BiVO_4$/RGO dispersion in the dark and under visible light irradiation: (A) in methanol dispersion for DMPO-$^{\bullet}O_2^-$; (B) in aqueous dispersion for DMPO-$^{\bullet}OH$ and (C) in aqueous dispersion for TEMPO-h^+.

of spin-trapped TEMPO-h^+ (Fig. 12C) for $Ag/Ag_3PO_4/BiVO_4$/RGO in dark condition was so strong, while it decreased to a greater extent when exposed to visible light irradiation, and almost no signal at the irradiation of 12 min. The result validated that holes should also contribute to the enhancement of photocatalytic performance. Thus, it is to say, h^+ and $^{\bullet}O_2^-$ were the main active species participating in the photocatalytic system, which was well consistent with the trapping experiments.

It is generally acknowledged that a desirable photocatalytic performance achieved by a photocatalyst could be ascribed to the following reasons: high surface area, superior absorption capability and higher separation efficiency of electron-hole pairs. In the case of $Ag/Ag_3PO_4/BiVO_4$/RGO nanocomposite hybrids, the above-mentioned advantages had been confirmed by the characterization technologies: BET, DRS, PL, PC and EIS tests. On the basis of the above experimental data and theoretical analysis, a synergistic mechanism for the TC degradation over $Ag/Ag_3PO_4/BiVO_4$/RGO nanocomposite was proposed, and represented in Scheme 1. The relative positions of energy bands of Ag_3PO_4 (2.39 eV) and $BiVO_4$ (2.4 eV) were known according to the results in the previous reports [15,22]. The CB and VB potentials of $BiVO_4$ were estimated to be +0.46 eV and +2.86 eV, while for Ag_3PO_4, they were 0.27 eV and 2.66 eV, respectively. In the previous report [16,18], the authors suggested that $Ag_3PO_4/BiVO_4$ composite followed a double-transfer mechanism under visible light irradiation, which implied that photo-generated electrons in the CB of Ag_3PO_4 would transfer to that of $BiVO_4$ and holes accumulated on the VB of Ag_3PO_4. Compared with pure $BiVO_4$ and Ag_3PO_4, the recombination of electron-hole pairs was greatly enhanced. However, the electrons left in Ag_3PO_4 or the holes left in $BiVO_4$ might easily recombine with the hole or electrons, respectively [46]. The introduction of metal Ag could show its contribution in the separation of electron-hole pairs, due to the forming Z-scheme heterojunction. He et al. reported that an efficient photocatalyst, $Ag_3PO_4/g\text{-}C_3N_4$, believed to follow a Z-scheme mechanism in the presence of metallic Ag, further to lead to a higher photocatalytic performance [19]. Herein, the introduction of metal Ag in $Ag_3PO_4/BiVO_4$ composite could facilitate a Z-scheme heterojunction. Metal Ag could play an important role in constructing a cross-linking bridge for two semiconductors [47,48]. The photo-induced electrons from $BiVO_4$ and holes from Ag_3PO_4 could be quickly transferred to Ag, which could bring about the activation of two substrates towards electron-rich and electron-deficient intermediates, respectively. Therefore an effective charge separation could be achieved, resulting in enhanced photoactivity. Furthermore, on one part, the presence of graphene into the above Z-scheme heterojunction $Ag_3PO_4/Ag/BiVO_4$ could effectively increase the surface area for holding more pollutants and reaction interspace. On the other part, graphene could play a vital role in capturing and shuttling electrons as an electron reservoir and the same role had also be proposed by previous investigations [29]. As a result, under visible light irradiation, both Ag_3PO_4 and $BiVO_4$ could be excited and produced electron-hole pairs due to their relatively narrow energy band gaps. The transfer of photo-induced electrons from $BiVO_4$ and holes from Ag_3PO_4 could be accelerated with the addition of graphene. The accumulated electrons in CB of Ag_3PO_4 could capture the dissolved O_2 and formed an oxidizing species: $^{\bullet}O_2^-$, which could participate in TC degradation in the photo-degradation system. Moreover, a slight of photo-generated electrons of $BiVO_4$ could transfer to GR and stored with GR, leading to the inhibition of photo-generated electrons and holes to a greater degree. The photo-generated holes left on the VB of $BiVO_4$ could directly decompose the target pollutant TC under visible light irradiation. So the enhancement of photocatalytic performance and photostability by $Ag/Ag_3PO_4/BiVO_4$/RGO should be attributed to the coupling effects of RGO and Ag/Ag_3PO_4 in the hybrid.

4. Conclusions

In summary, graphene-bridged $Ag_3PO_4/Ag/BiVO_4$ (040) Z-scheme photocatalyst was prepared by a hierarchical assembly procedure, which combined with an in situ precipitation and a photo-reduction method. The as-prepared $Ag/Ag_3PO_4/BiVO_4$/RGO nanocomposites exhibited excellent photocatalytic activity for TC degradation under visible light irradiation, which was much faster than those over pure Ag_3PO_4, $BiVO_4$ and other composites. Sev-

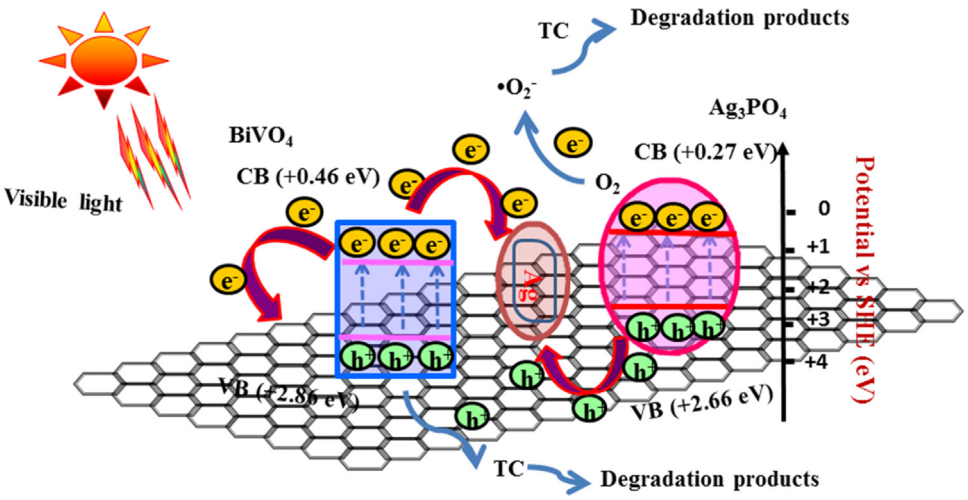

Scheme 1. Schematic illustration of the proposed mechanism for photo-generated charge carrier transfer in the $Ag/Ag_3PO_4/BiVO_4$/RGO nanocomposite under visible light irradiation (black sheet represents graphene in the diagram).

eral parameters: catalytic behavior, catalysis dosage, initial TC concentrations, reaction pH, light irradiation condition, supporting electrolytes and water sources were taken into discussion. The results demonstrated that $Ag/Ag_3PO_4/BiVO_4$/RGO showed the optimal photocatalytic performance with catalysis dosage at ca. 0.5 g/L, pH at ca. 6.75 and Na_2SO_4 (0.5 M) as the supporting electrolyte. The enhanced photocatalytic performance should be beneficial for the cocatalytic effects of Ag/Ag_3PO_4 and RGO, which could lead to higher surface area, more desirable absorption capability and higher separation efficiency of photo-generated electron-hole pairs. Moreover, Ag/Ag_3PO_4 and RGO could be used as protective coatings that partially inhibited the photocorrosion of single semiconductor, especially pure Ag_3PO_4, thus the $Ag/Ag_3PO_4/BiVO_4$/RGO composite also displayed superior photostability. Most importantly, high degradation efficiencies were also achieved by $Ag/Ag_3PO_4/BiVO_4$/RGO in the degrading TC from medical wastewater, municipal wastewater, river wastewater and tap wastewater, suggesting its satisfying application potential in future wastewater treatment. This study inspires the exploration of similar facile methods to stabilize other easily photo-corroded photocatalysts for better applications in addressing environmental protection issues.

Acknowledgments

This research was financially supported by the project of National Natural Science Foundation of China (NSFC) (Nos. 51378188, 51478170, 51508178), Doctoral Fund of Ministry of Education of China (20130161120021) and Planned Science and Technology Project of Hunan Province, China (No. 2015SK20672).

References

[1] G.M. Zeng, M. Chen, Z.T. Zeng, Risks of neonicotinoid pesticides, Science 340 (2013) 1403.
[2] B.F. Luo, D.B. Xu, D. Li, G.L. Wu, M.M. Wu, W.D. Shi, M. Chen, Fabrication of a Ag/Bi_3TaO_7 plasmonic photocatalyst with enhanced photocatalytic activity for degradation of tetracycline, ACS Appl. Mater. Interfaces 7 (2015) 17061–17069.
[3] S. Reardon, Antibiotic resistance sweeping developing world, Nature 509 (2014) 141–142.
[4] S. Rodriguez-Mozaz, S. Chamorro, E. Marti, B. Huerta, M. Gros, A. Sanchez-Melsio, C.M. v Borrego, D. Barcelo, J.L. Balcazar, Occurrence of antibiotics and antibiotic resistance genes in hospital and urban wastewaters and their impact on the receiving river, Water Res. 69 (2015) 234–242.
[5] A.L. Ling, N.R. Pace, M.T. Hernandez, T.M. LaPara, Tetracycline resistance and class 1 integron genes associated with indoor and outdoor aerosols, Environ. Sci. Technol. 47 (2013) 4046–4052.
[6] J. Tolls, Sorption of veterinary pharmaceuticals in soils: a review, Environ. Sci. Technol. 35 (2001) 3397–3406.
[7] D.W. Kolpin, E.T. Furlong, M.T. Meyer, E.M. Thurman, S.D. Zaugg, L.B. Barber, H.T. Buxton, Pharmaceuticals, hormones, and other organic wastewater contaminants in U.S. streams, 1999–2000: a national reconnaissance, Environ. Sci. Technol. 36 (2002) 1202–1211.
[8] X. Miao, F. Bishay, M. Chen, Metcalfe, Occurrence of antimicrobials in the final effluents of wastewater treatment plants in Canada, Environ. Sci. Technol. 38 (2004) 3533–3541.
[9] L.L. Ji, W. Chen, L. Duan, D.Q. Zhu, Mechanisms for strong adsorptionof tetracycline to carbon nanotubes: a comparative study using activated carbon and graphite as adsorbents, Environ. Sci. Technol. 43 (2009) 2322–2327.
[10] H. Wang, X.Z. Yuan, Y. Wu, G.M. Zeng, H.R. Dong, X.H. Chen, In situ synthesis of In_2S_3@MIL-125(Ti) core-shell microparticle for the removal of tetracycline from wastewater by integrated adsorption and visible-light-driven photocatalysis, Appl. Catal. B: Environ. 186 (2016) 19–29.
[11] K. Baransi, Y. Dubowski, I. Sabbah, Synergetic effect between photocatalytic degradation and adsorption processes on the removal of phenolic compounds from olive mill wastewater, Water Res. 46 (2012) 789–798.
[12] I. El Saliby, L. Erdei, J.H. Kim, H.K. Shon, Adsorption and photocatalytic degradation of methylene blue over hydrogen–titanate nanofibres produced by a peroxide method, Water Res. 47 (2013) 4115–4125.
[13] N.C. Castillo, A. Heel, T. Graule, C. Pulgarin, Flame-assisted synthesis of nanoscale amorphous and crystalline, spherical $BiVO_4$ with visible-light photocatalytic activity, Appl. Catal. B: Environ. 95 (2010) 335–347.
[14] W.H. Feng, B. Wang, Z.Y. Zheng, Z.B. Fang, Z.F. Wang, S.Y. Zhang, Y.H. Li, P. Liu, Predictive model for optimizing the near-field electromagnetic energy transfer in plasmonic nanostructure-involved photocatalysts, Appl. Catal. B: Environ. 186 (2016) 143–150.
[15] X.H. Gao, H.B. Wu, L.X. Zheng, Y.J. Zhong, Y. Hu, X.W. Lou, Formation of mesoporous heterostructured $BiVO_4/Bi_2S_3$ hollow giscoids with enhanced photoactivity, Angew. Chem. Int. Ed. 53 (2014) 5917–5921.
[16] Q. Yuan, L. Chen, M. Xiong, J. He, S.L. Luo, C.T. Au, Shuang-Feng Yin, $Cu_2O/BiVO_4$ heterostructures: synthesis and application in simultaneous photocatalytic oxidation of organic dyes and reduction of Cr(VI) under visible light, Chem. Eng. J. 255 (2014) 394–402.
[17] Y. Hu, D.Z. Li, Y. Zheng, W. Chen, Y.H. He, Y. Shao, X.Z. Fu, G.C. Xiao, $BiVO_4/TiO_2$ nanocrystalline heterostructure: a wide spectrum responsive photocatalyst towards the highly efficient decomposition of gaseous benzene, Appl. Catal. B: Environ. 104 (2011) 30–36.
[18] C.J. Li, P. Zhang, R. Lv, J.W. Lu, T. Wang, S.P. Wang, H.F. Wang, J.L. Gong, Selective deposition of Ag_3PO_4 on monoclinic $BiVO_4$ (040) for highly efficient photocatalysis, Small 9 (2013) 3951–3956.
[19] Y.M. He, L.H. Zhang, B.T. Teng, M.H. Fan, New application of Z-scheme $Ag_3PO_4/g\text{-}C_3N_4$ composite in converting CO_2 to fuel, Environ. Sci. Technol. 49 (2015) 649–656.
[20] W.Z. Chen, Z. Wang, X.F. Zhang, High-efficiency visible-light-driven Ag_3PO_4/AgI photocatalysts: Z-scheme photocatalytic mechanism for their enhanced photocatalytic activity, J. Phys. Chem. C 117 (2013) 19346–19352.
[21] H.L. Lin, J. Cao, B.D. Luo, B.Y. Xu, S.F. Chen, Synthesis of novel Z-scheme AgI/Ag/AgBr composite with enhanced visible light photocatalytic activity, Catal. Commun. 21 (2012) 91–95.

[22] Y.Y. Bu, Z.Y. Chen, C.J. Sun, Highly efficient Z-scheme Ag_3PO_4/Ag/WO_{3-x} photocatalyst for its enhanced photocatalytic performance, Appl. Catal. B: Environ. 179 (2015) 363–371.
[23] J. Li, S.K. Cushing, P. Zheng, T. Senty, F. Meng, A.D. Bristow, A. Manivannan, N. Wu, Solar hydrogen generation by a CdS-Au-TiO_2 sandwich nanorod array enhanced with Au nanoparticle as electron relay and plasmonic photosensitizer, J. Am. Chem. Soc. 136 (2014) 8438–8449.
[24] X.F. Yang, J.L. Qin, Y. Jiang, R. Li, Y. Li, H. Tang, Bifunctional TiO_2/Ag_3PO_4/graphene composites with superior visible light photocatalytic performance and synergistic inactivation of bacteria, RSC Adv. 4 (2014) 18627–18636.
[25] Y. Hou, F. Zuo, Q. Ma, C. Wang, P.Y. Feng, Ag_3PO_4 oxygen evolution photocatalyst employing synergistic action of Ag/AgBr nanoparticles and graphene sheets, J. Phys. Chem. C 116 (2012) 20132–20139.
[26] Q.J. Xiang, J.G. Yu, M. Jaroniec, Graphene-based semiconductor photocatalysts, Chem. Soc. Rev. 41 (2012) 782–796.
[27] F. Chen, Q. Yang, Y. Zhong, H.X. An, J.W. Zhao, T. Xie, Photo-reduction of bromate in drinking water by metallic Ag and reduced graphene oxide (RGO) jointly modified BiVO4 under visible light irradiation, Water Res. 101 (2016) 555–563.
[28] V. Stengl, D. Popelkova, P. Vlacil, TiO_2-graphene nanocomposite as high performace photocatalysts, J. Phys. Chem. C 115 (2011) 25209–25218.
[29] J.X. Wang, P.X. Wang, Y.T. Cao, J. Chen, W.J. Li, Y. Shao, Y. Zheng, D.Z. Li, A high efficient photocatalyst Ag_3VO_4/TiO_2/graphene nanocomposite with wide spectral response, Appl. Catal. B: Environ. 136–137 (2013) 94–102.
[30] H.Y. Li, Y.J. Sun, B. Cai, S.Y. Gan, D.X. Han, L. Niu, T.S. Wu, Hierarchically Z-scheme photocatalyst of Ag@AgCl decorated on $BiVO_4$ (040) with enhancing photoelectrochemical and photocatalytic performance, Appl. Catal. B: Environ. 170–171 (2015) 206–214.
[31] A.Y. Booshehri, S.C. Goh, J.D. Hong, R.R. Jiang, R. Xu, Effect of depositing silver nanoparticles on $BiVO_4$ in enhancing visible light photocatalytic inactivation of bacteria in water, J. Mater. Chem. A 2 (2014) 6209.
[32] P.H. Wang, Y.X. Tang, Z.L. Dong, Z. Chen, T.T. Lim, Ag-AgBr/TiO_2/RGO nanocomposite for visible-light photocatalytic degradation of penicillin G, J. Mater. Chem. A 1 (2013) 4718.
[33] H. Liu, W.R. Cao, Y. Su, Y. Wang, X.H. Wang, Synthesis characterization and photocatalytic performance of novel visible-light-induced Ag/BiOI, Appl. Catal. B: Environ. 111–112 (2012) 271–279.
[34] T. Wang, C.J. Li, J.Y. Ji, Y.J. Wei, P. Zhang, S.P. Wang, X.B. Fan, J.L. Gong, Reduced graphene oxide (rGO)/$BiVO_4$ composites with maximized interfacial coupling for visible light photocatalysis, ACS Sustainable Chem. Eng. 2 (2014) 2253–2258.
[35] H. Zhang, L.H. Guo, D.B. Wang, L.X. Zhao, B. Wan, Light-induced efficient molecular oxygen activation on a Cu(II)-grafted TiO_2/graphene photocatalyst for phenol degradation, ACS Appl. Mater. Interfaces 7 (2015) 1816–1823.
[36] Y.Y. Bu, Z.Y. Chen, Role of polyaniline on the photocatalytic degradation and stability performance of the polyaniline/silver/silver phosphate composite under visible light, ACS Appl. Mater. Interfaces 6 (2014) 17589–17598.
[37] C. Cai, Z.Y. Zhang, J. Liu, N. Shan, H. Zhang, Visible light-assisted heterogeneous Fenton with $ZnFe_2O_4$ for the degradation of Orange II in water, Appl. Catal. B: Environ. 182 (2016) 456–468.
[38] F. Chen, Q. Yang, C.G. Niu, X.M. Li, C. Zhang, J.W. Zhao, Enhanced visible light photocatalytic activity and mechanism of $ZnSn(OH)_6$ nanocubes modified with AgI nanoparticles, Catal. Commun. 73 (2016) 1–6.
[39] M. Rezaei, A. Habibi-Yangjeh, Simple and large scale refluxing method for preparation of Ce-doped ZnO nanostructures as highly efficient photocatalyst, Appl. Surf. Sci. 265 (2013) 591–596.
[40] H. Wang, X.Z. Yuan, Y. Wu, G.M. Zeng, X.H. Chen, L.J. Leng, H. Li, Synthesis and applications of novel graphitic carbon nitride/metal-organic frameworks mesoporous photocatalyst for dyes removal, Appl. Catal. B: Environ. 174 (2015) 445–454.
[41] B. Zhou, X. Zhao, H.J. Liu, J.H. Qu, C.P. Huang, Visible-light sensitive cobalt-doped $BiVO_4$ (Co-$BiVO_4$) photocatalytic composites for the degradation of methylene blue dye in dilute aqueous solutions, Appl. Catal. B: Environ. 99 (2010) 214–221.
[42] J.J. López-Penalver, M. Sánchez-Polo, C.V. Gómez-Pacheco, J. Rivera-Utrilla, Photodegradation of tetracyclines in aqueous solution by using UV and UV/H_2O_2 oxidation processes, J. Chem. Technol. Biotechnol. 85 (2010) 1325–1333.
[43] H. Xiao, R.P. Liu, X. Zhao, J.H. Qu, Enhanced degradation of 2,4-dinitrotoluene by ozonation in the presence of manganese(II) and oxalic acid, J. Mol. Catal. A: Chem. 286 (2008) 149–155.
[44] H.Q. Sun, G.L. Zhou, Y.X. Wang, A. Suvorova, S.B. Wang, A new metal-free carbon hybrid for enhanced photocatalysis, ACS Appl. Mater. Interfaces 6 (2014) 16745–16754.
[45] X. Zhang, T. Guo, X. Wang, Y. Wang, C. Fan, H. Zhang, Facile composition-controlled preparation and photocatalytic application of BiOCl/$Bi_2O_2CO_3$ nanosheets, Appl. Catal. B: Environ. 150–151 (2014) 486–495.
[46] S.F. Chen, W. Zhao, W. Liu, H.Y. Zhang, X.L. Yu, Y.H. Chen, Preparation, characterization and activity evaluation of p–n junction photocatalyst p-ZnO/n-TiO_2, J. Hazard. Mater. 172 (2009) 1415–1423.
[47] J.X. Wang, H. Ruan, W.J. Li, D.Z. Li, Y. Hu, J. Chen, Y. Shao, Y. Zheng, Highly efficient oxidation of gaseous benzene on novel Ag_3VO_4/TiO_2 nanocomposite photocatalysts under visible and simulated solar light irradiation, J. Phys. Chem. C 116 (2012) 13935–13943.
[48] M. Xu, L. Han, S.j. Dong, Facile fabrication of highly efficient g-C_3N_4/Ag_2O heterostructured photocatalysts with enhanced visible-light photocatalytic activity, ACS Appl. Mater. Interfaces 5 (2013) 12533–12540.